Modelling the waviness of the fibres in non-crimp fabric composites using 3D finite element models with straight tows

Authors: Luis Miguel Ferreira (corresponding author), Enrique Graciani, Federico París

Affiliation (for all authors): Grupo de Elasticidad y Resistencia de Materiales, Escuela Técnica Superior de Ingenieros, Universidad de Sevilla.

Address (for all authors):
Grupo de Elasticidad y Resistencia de Materiales.
Escuela Técnica Superior de Ingenieros, Universidad de Sevilla.
Camino de los Descubrimientos s/n.
41092 Sevilla, España
Phone: +34 954 487 300
Fax: +34 954 461 637
Email: luismmferreira@ipt.pt (Luis Miguel Ferreira), egraciani@us.es (Enrique Graciani), fparis@us.es (Federico París).

Abstract

A new approach to efficiently model the waviness of the fibres in non-crimp fabric (NCF) composites using mesoscale 3D finite element (FE) models with straight tows is presented. This approach omits the geometric curvature of the tows allowing the use of a straight 3D FE mesh, the waviness of the fibres being taken into account with the definition of the mechanical properties of each element according to the actual direction of the fibres. A representative unit cell (RUC) of a single NCF lamina with fibre crimp has been developed following this approach. The RUC has been used to predict the stiffness properties and to study the stresses/strains that develop along the length of the tows. To ensure the validity of the new modelling approach, the results obtained with its use have been compared with the results obtained from an equivalent RUC in which the FE mesh follows the actual curvature of the tows, in accordance with the classical modelling approach. The results show that the new approach is a valid alternative to model the waviness of the fibres, both in terms of simplicity in modelling and accuracy of the results, opening up the possibility of studying damage mechanisms more efficiently.

Keywords
Composites; Non-crimp fabric (NCF); Finite element model (FEM); Finite element analysis (FEA); Mechanical properties; Fibre waviness.

1. Introduction

The need for an alternative to unidirectional pre-impregnated tape in high-performance composites applications led to the appearance of non-crimp fabric (NCF) composites [1] which present an intermediate through thickness behaviour between unidirectional pre-impregnated tape and woven fabrics [2]. These new composites are made from dry preforms that consist of layers of straight fibre tows (or tows for short) held in position by a stitching yarn creating a theoretical crimpless fabric, see Fig. 1. The use of dry NCF preforms involves lower cost and faster manufacturing techniques, than those associated with the use of pre-impregnated preforms. In practice, however, the NCF composites present a complicated internal structure with several geometrical features at the mesoscopic scale, such as resin pockets between the tows and some in-plane and out-of-plane fibre waviness that are introduced in the different stages of the manufacturing process [3, 4]. These features are closely related to the final mechanical performance of the NCF composites. It is therefore essential to characterize them in order to predict the macroscale mechanical properties of the NCF composites by means of meso-mechanical models.

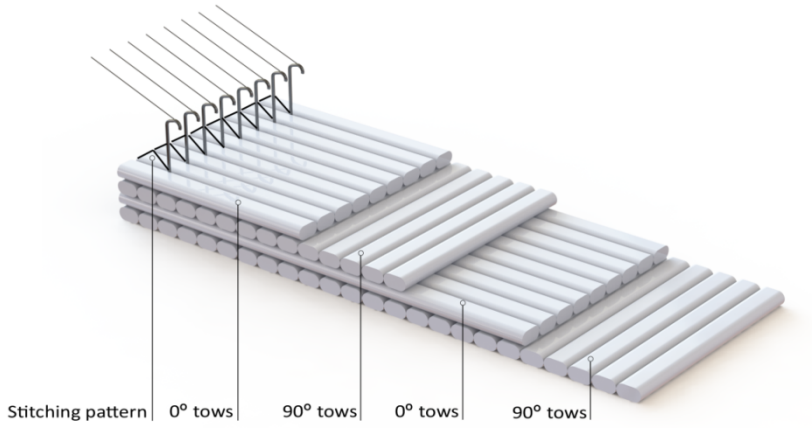

Fig. 1. Representation of an NCF preform.

The aforementioned imperfections in the internal structure of an NCF composite can be observed in Fig. 2, where the resin pockets and the slight crimp of the tows in particular appear clearly reflected.

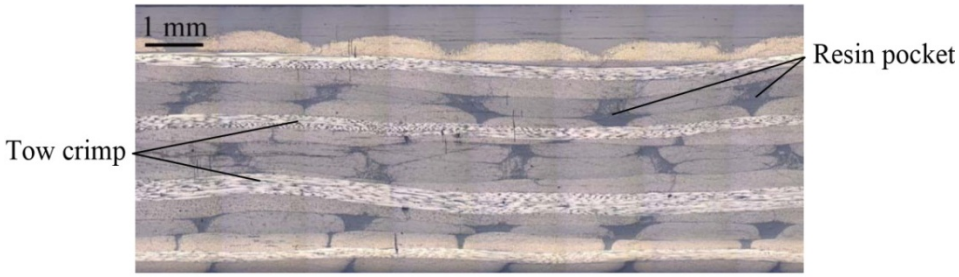

Fig. 2. Cross-section of a typical NCF composite [5].

Although it is possible to perform representative studies of NCF composites with a 2D approach [6-8], the complex mesoscopic architecture of these materials is not completely represented by them [9], since it is highly irregular along any direction of the material. On the other hand, 3D finite element (FE) models that take into account the waviness of the tows, either in-plane or out-of-plane, are very difficult to generate [10-15]. Additionally, due to the complexity of the architecture and to the large number of elements required in the FE mesh, these models are also very expensive from a computational point of view. Moreover, the work needed to generate the 3D FE models increases further if parametric capabilities are incorporated. Accordingly, some authors have chosen to use 3D FE models of NCF laminates with straight tows and with a rectangular cross-section [10, 13, 14, 16].

In order to overcome most of the limitations described above, a new approach for modelling the waviness of the fibres in 3D FE models with straight tows is presented in this paper. This new modelling approach is described and compared with the classical modelling approach [11] in Section 2. For this purpose, a representative unit cell (RUC) of a single NCF lamina with fibre crimp has been generated. The fibre crimp has been modelled in accordance with the new modelling approach (see Section 2.1) and with the classical modelling approach (see Section 2.2). The stiffness properties of the constituents are described in Section 2.3. Next, in Section 3, the apparent in-plane stiffness properties of both numerical models are compared for different fibre crimp angles. The stresses and strains that develop along the tows length, in global and material systems, for both numerical models when submitted to a pure tensile strain in the nominal fibre direction are studied and compared in Section 4. Finally, the conclusions are set out in Section 5.

2. Numerical models

The classical representation of the internal structure of an NCF composite such as that observed in Fig. 2 by a model (in 2D for simplicity) is shown in Fig. 3(a). The tow appears curved as it is in reality, and the fibres change the orientation in accordance with the orientation of the tow [6, 7, 11]. The curved part of the tow is schematically represented in Fig. 3(b) and one curved element is represented isolated in Fig. 3(c), indicating specifically the direction of the fibres. Notice that α is the angle between the fibre direction 1 and the global direction x and will be referred to as *misorientation angle* in the following. From a computational point of view the 3D FE mesh is obtained extruding the cross section of the tow along a path that includes both the length of the tow that it is straight and the waviness considered.

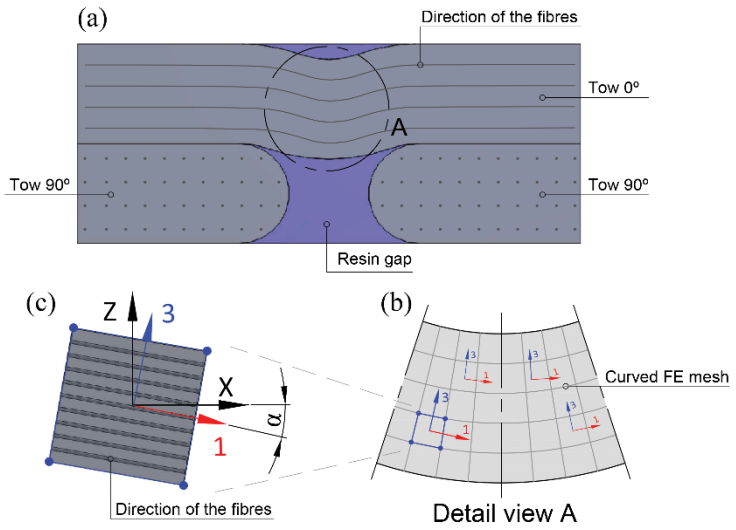

Fig. 3. Classical 2D representation of the internal structure of an NCF composite: (a) NCF composite with fibre crimp, (b) detail view of the fibre crimp, (c) isolated curved element.

The alternative that is going to be studied in this paper is to omit the geometrical curvature of the tow, while taking into consideration the waviness of the fibres, see Fig. 4(a). The use of straight tows obviously permits the use of a straight FE mesh, as represented in Fig. 4(b). An isolated element is represented with the appropriate orientation of the fibres in Fig. 4(c).

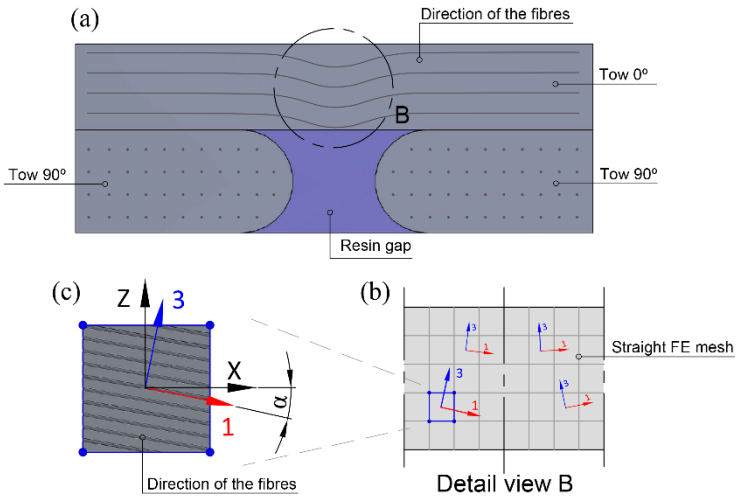

Fig. 4. Alternative 2D representation of the internal structure of an NCF composite: (a) NCF composite with fibre crimp, (b) detail view of the fibre crimp, (c) isolated straight element.

Following the two approaches described above, 3D FE models of the RUC of a single NCF lamina with different fibre crimp angles have been generated. However, prior to their presentation it is important to define the process used to obtain them. The RUC corresponds to the minimum unit cell that, repeated through its plane, will generate a

complete lamina with all its tows oriented along the same direction. This concept is illustrated in Fig. 5.

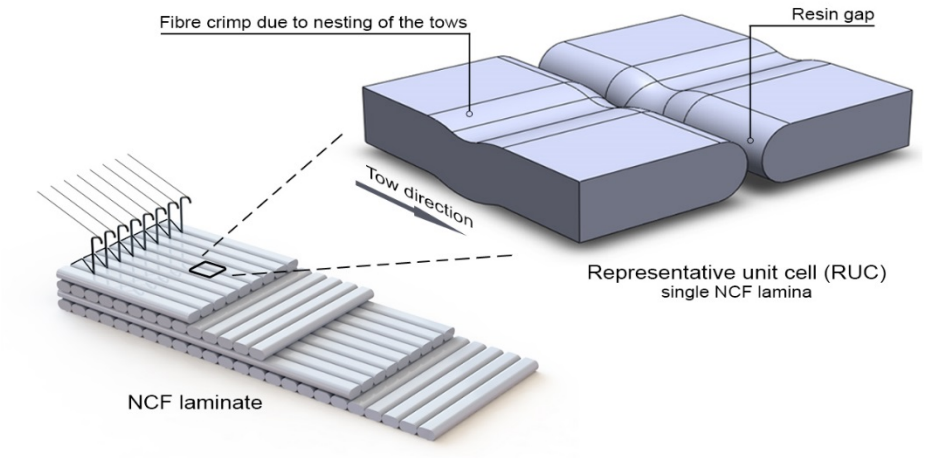

Fig. 5. Process used to obtain the representative unit cell of a single NCF lamina.

2.1. Single NCF lamina with fibre crimp modelled in a straight 3D FE mesh (New Modelling Approach)

Mesoscopic scale 3D FE models of the RUC of a single NCF lamina with different fibre crimp angles have been generated with a straight mesh, following the new modelling approach represented in Fig. 4. The tows have been modelled as a homogenous material (without considering their microscopic constituents: fibre and matrix) with linear transversely isotropic behaviour, the isotropic plane being perpendicular to the fibres, and the resin pockets have been modelled as a homogeneous isotropic material filling the free spaces between the tows.

The unit cell developed contains two half tows and a resin pocket is left between them, see Fig. 6(a). The resin has been removed in Fig. 6(b) for a better understanding of the size, shape and orientation of the tows.

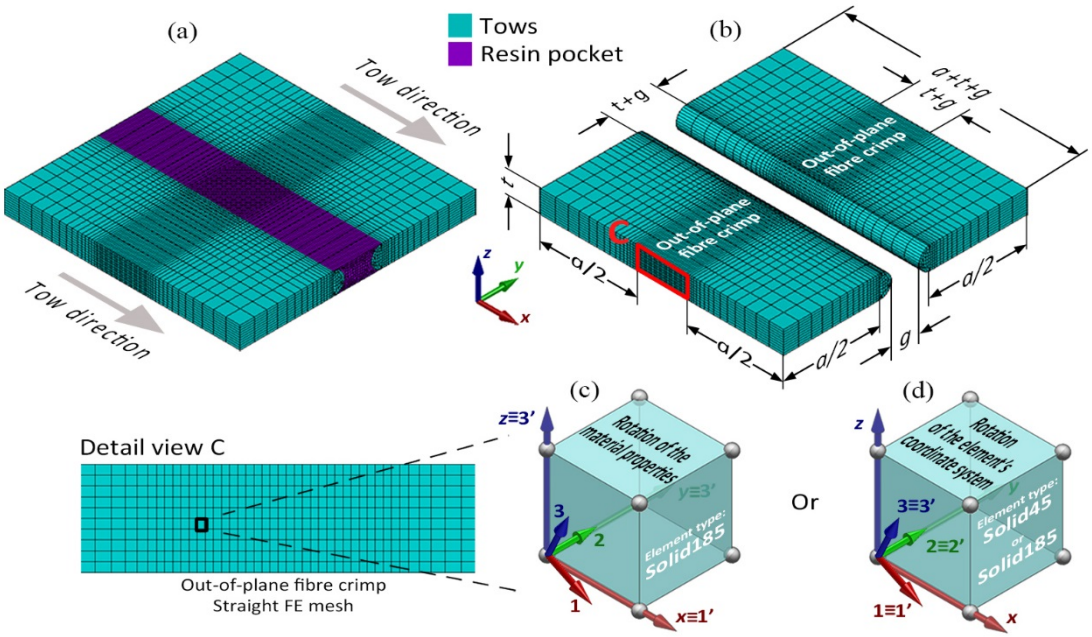

Fig. 6. 3D FE model of the RUC of a single NCF lamina with the fibre crimp modelled in a straight mesh: (a) complete lamina model, (b) tow shape and dimensions employed, (c) rotation of the material properties, (d) rotation of the element's coordinate system.

The geometrical parameters employed are shown in Fig. 6(b), where *a* represents the length of the tow not affected by the crimp, *t* the thickness of the lamina and *g* the width of the gap left between two adjacent tows of the lamina.

The average fibre volume fraction of the lamina V_f^l has been calculated from the average fibre volume fraction of the tows V_f^t and the relative dimensions of the cross-sections of the tow A_t and of the lamina A_l. Assuming that the two sides of the cross-section of the tow are semi-circular, Eq. (1) relates V_f^l with V_f^t and with the geometrical parameters *a*, *t* and *g*.

$$V_f{}^l = V_f{}^t \frac{A^t}{A^l} = \frac{2V_f{}^t \left(t\frac{a}{2} + \pi\frac{t^2}{4} \right)}{t\left(a+t+g\right)} \tag{1}$$

The values of the parameters *a*, *t*, *g* and V_f^t, summarized in Table 1, have been obtained for a lamina fibre volume fraction of 60%. The results of the microstructure characterization measured in [17, 18] have been taken into account to estimate the FE model dimensions.

a (mm)	t (mm)	g (mm)	V_f^t
2.06	0.24	0.30	69%

Table 1. Values considered for the parameters a, t, g and V_f^t for $V_f^l = 60\%$.

In accordance with the global coordinate system *xyz* represented in Fig. 6, the plane of the lamina is the *xy*-plane and *z* is the through-thickness direction. The local coordinate system 123 corresponds to the actual direction of the fibres and the local coordinate system 1'2'3' is employed to express the material properties of the tows.

Two possibilities have been considered to model the fibre crimp in a straight 3D FE mesh. In the first one, the local coordinate system 1'2'3' employed to define the material properties is parallel to the global coordinate system *xyz* and an appropriate definition of anisotropic material properties is carried out in each element to take into account the fibre crimp, see Fig. 6(c). This procedure is described in Section 2.1.1. In the second one, the local coordinate system 1'2'3' is rotated in each element to align direction 1' with the fibre's direction 1, see Fig. 6(d). Therefore identical transversely isotropic material properties are employed in all elements. This procedure is detailed in Section 2.1.2.

Defining β as an angular parameter that corresponds to the maximum misorientation angle α and thus represents the maximum fibre crimp, several maximum crimp angles, in a range of 3º to 15º, have been considered for the purpose of evaluating the validity of the approach. The values of $\alpha(x)$ along the tow length for $\beta = 3º, 9º$ and 15º, are shown in Fig. 7.

In this study, only an out-of-plane rotation of the fibre around the global *y*-axis, α, has been considered. Moreover, a simplified evolution of the fibre crimp $\alpha(x)$, detailed above, has been assumed. However, the methodology can be easily extended for any evolution $\alpha(x, y, z)$ of the waviness of the fibres around the *y*-axis or to include rotations around the *z*-axis (in-plane waviness).

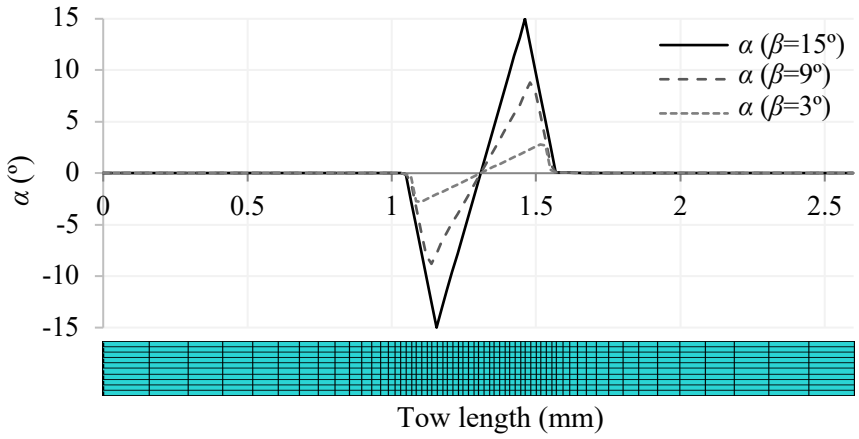

Fig. 7. Variation of the misorientation angle α for β=3º, 9º and 15º along the length of the tows.

The FE code used has been ANSYS® [19] and linear solid elements SOLID45 or SOLID185 (depending on the procedure used for modelling the fibre crimp) with eight nodes and three degrees of freedom at each node have been considered. As an indication, the complete unit cell has been defined with 35760 elements and 40321 nodes.

2.1.1. Rotation of the material properties (Anisotropic material)

One of the procedures employed for the modelling of the fibre crimp with a straight 3D FE mesh is by means of the rotation of the material properties into the element coordinate system 1'2'3', which is parallel to the global coordinate system *xyz*, see Fig. 6(c). This will cause the appearance of anisotropic material properties due to the rotation of the behaviour law from the transversely isotropic material of the tows into global coordinates.

The transformation for stresses and strains [20] is given by

$$\boldsymbol{\sigma} = \boldsymbol{T}^{-1}\boldsymbol{\sigma}^{*} \quad \text{and} \quad \boldsymbol{\varepsilon} = \boldsymbol{T}^{T}\boldsymbol{\varepsilon}^{*}, \tag{2}$$

in which $\boldsymbol{T}$ is the orthogonal transformation matrix (see Appendix A), $\boldsymbol{\sigma}$ and $\boldsymbol{\varepsilon}$ are the stresses and strains in the global coordinate system *xyz* and $\boldsymbol{\sigma}^{*}$ and $\boldsymbol{\varepsilon}^{*}$ are the stresses and strains in the local coordinate system 123.

Knowing that stresses and strains in the local coordinate system are related by the transversely isotropic constitutive law $\boldsymbol{\sigma}^{*} = \boldsymbol{C}^{*}\boldsymbol{\varepsilon}^{*}$ or $\boldsymbol{\varepsilon}^{*} = \boldsymbol{S}^{*}\boldsymbol{\sigma}^{*}$, the transformation from local to global coordinate system results in the anisotropic constitutive law $\boldsymbol{\sigma} = \boldsymbol{C}\boldsymbol{\varepsilon}$ or $\boldsymbol{\varepsilon} = \boldsymbol{S}\boldsymbol{\sigma}$.

Therefore, the transformation laws for the elastic stiffness $\boldsymbol{C}$ and elastic compliance $\boldsymbol{S}$ of the material in the global coordinate system are

$$\boldsymbol{C} = \boldsymbol{T}^{-1}\boldsymbol{C}^{*}\left(\boldsymbol{T}^{-1}\right)^{\boldsymbol{T}} \text{ and } \boldsymbol{S} = \boldsymbol{T}^{\boldsymbol{T}}\boldsymbol{S}^{*}\boldsymbol{T} \tag{3}$$

This procedure requires the use of an element with anisotropic material capabilities, for example, the 3D structural solid element SOLID185 from the ANSYS® FE code [19].

The number of distinct anisotropic materials that have to be created corresponds to the number of different misorientation angles α.

2.1.2. Rotation of the element's coordinate system

In this procedure the fibre crimp is modelled with the rotation of the element's coordinate system 1'2'3' into the actual direction of the fibres 123, see Fig. 6(d). To apply this procedure a local coordinate system 1'2'3' has to be defined for each misorientation angle α. Next, the straight elements affected by the fibre crimp have to be selected and their coordinate system, which at this stage is aligned with the global direction *xyz,* is replaced by the corresponding local coordinate systems 1'2'3' and thus it will be aligned with the actual direction of the fibres 123.

Knowing that the element's coordinate system defines the direction of the material properties and that in this procedure it is aligned with the actual direction of the fibres, identical transversely isotropic material properties can be employed in all elements of the tows. This eliminates the need for the pre-processing stage to obtain the elastic stiffness $\boldsymbol{C}$ and elastic compliance $\boldsymbol{S}$ of the material for each misorientation angle α described in Section 2.1.1.

Two distinct 3D structural solid elements from ANSYS® FE code, SOLID185 or SOLID45, can be employed for modelling the fibre crimp with the rotation of the element's coordinate system [19]. However, SOLID45 presents some advantages when working with transversely isotropic material properties. Firstly, it enables the definition of a different bilinear stress-strain behaviour in transversely isotropic materials, while SOLID185 only allows a linear material behaviour to be defined. Another important advantage of using SOLID45 is found at the post-processing stage. While SOLID45 allows all stress and strain components in the global coordinate system *xyz* to be directly represented either in a specific local coordinate system 1'2'3' or in the actual direction of the fibres 123, SOLID185 only allows the direct representation of stress and strain components either in the global direction *xyz* or in a specific local coordinate system 1'2'3'. This is particularly relevant because given the existence of fibre crimp there may be areas within the tows of an NCF composite in which the stresses and strains in the actual direction of the fibres 123 may be quite different from their nominal values.

2.2. Single NCF lamina with fibre crimp modelled with a curved 3D FE mesh (Classical Modelling Approach)

In order to be able to validate the new modelling approach detailed in the previous section, an equivalent RUC of a single NCF lamina with fibre crimp due to nesting has been generated, see Fig. 8(a). In this unit cell the fibre crimp has been modelled with a curved FE mesh, that is, following the classical modelling approach represented in Fig. 3.

The geometrical parameters employed, shown in Fig. 8(b), are identical to those shown in Fig. 6(b), which are indicated in Table 1.

This approach requires the use of the 3D structural solid element SOLID45 from ANSYS® FE code [19] since it allows the definition of the element coordinate system 1'2'3' based on the element I-J side, see Fig. 8(c). Accordingly, the orthotropic material directions correspond to the element coordinate system 1'2'3' and thus to the actual direction of the fibres 123. Notice that this classical modelling approach for the fibre crimp was used in previous numerical studies of NCF composites [9, 11, 21] and woven composites [22].

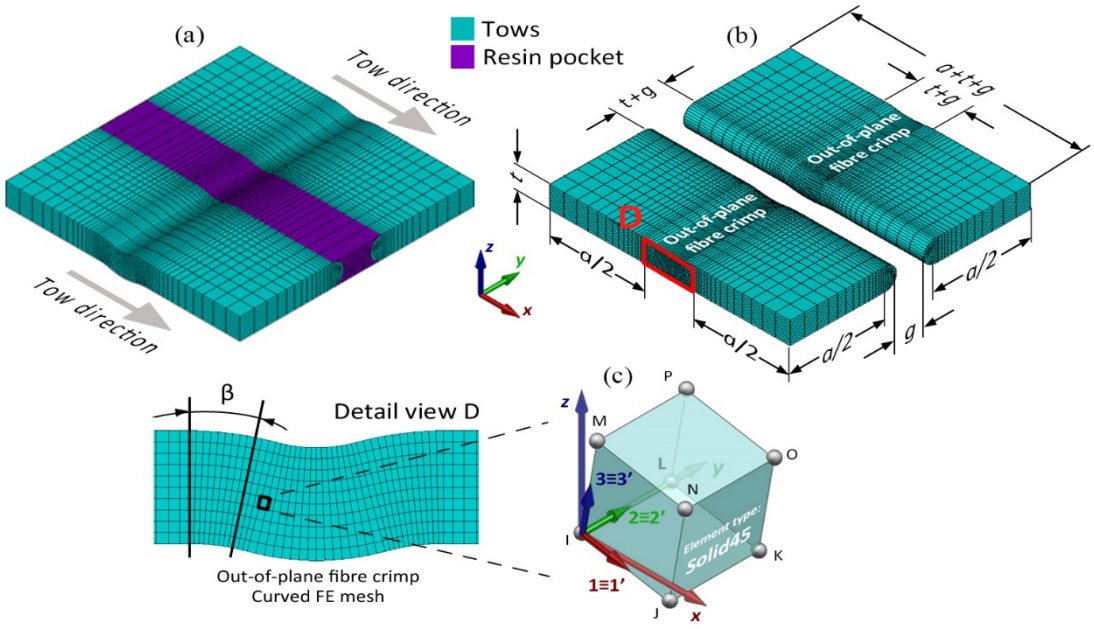

Fig. 8. 3D FE model of the RUC of the NCF lamina with fibre crimp modelled with a curved mesh: (a) complete lamina model, (b) tow shape with dimensions employed, (c) rotation of an element.

As an indication, the unit cell shown in Fig. 8(a) has been defined with 30912 elements and 34827 nodes.

2.3. Stiffness properties of the constituents

At the mesoscopic scale, the stiffness properties required to carry out the FE analysis are the stiffness properties of the resin pockets and of the tows. Since the tows are constituted by a large number of parallel fibres uniformly distributed and impregnated with a resin, their behaviour can be considered transversely isotropic (with elastic constants: E_{11}^t, ν_{12}^t, G_{12}^t, E_{22}^t, ν_{23}^t and G_{23}^t).

The FE models have been generated according to the NCF composites tested within the FALCOM project [14, 17, 23] but as no experimental measurements were performed to estimate the stiffness properties of the tows, the rule of mixtures has been employed as an averaging technique to estimate their values as a function of the elastic properties of the fibre and of the resin, see Table 2. The resin employed is characterized by a tensile modulus $E^m = 3.50$ GPa, a Poisson's ratio $\nu^m = 0.42$ and a corresponding shear modulus $G^m = 1.23$ GPa. Transversely isotropic carbon fibres are characterized by identical stiffness properties in all planes containing the fibre axis: $E_{11}^f = 237$ GPa, $\nu_{12}^f = 0.25$ and $G_{12}^f = 94.8$ GPa. Notice that according to the rule of mixtures, the values of the elastic constants in the planes normal to the fibre axis $\left(E_{22}^f,\ \nu_{23}^f \text{ and } G_{23}^f\right)$ are not needed to estimate the apparent stiffness properties of the tows either in the longitudinal plane or in the transverse planes, see Appendix B.

V_f^t	$E_{11}^t(GPa)$	$E_{22}^t(GPa)$	ν_{12}^t	ν_{23}^t	$G_{12}^t(GPa)$	$G_{23}^t(GPa)$
60%	165.5	11.43	0.30	0.42	4.03	4.03

Table 2. Stiffness properties of the tows obtained with the rule of mixtures.

In the following section, the apparent in-plane stiffness properties of a single NCF lamina are estimated for different fibre crimp angles using the 3D FE models generated following both approaches. The results obtained with the new modelling approach are compared with the results obtained with the classical modelling approach in order to assess its validity. It should be noted that an RUC identical to the one presented in Section 2.2, which follows the classical modelling approach of the fibre crimp, was used in [11] to predict the apparent in-plane stiffness properties of NCF laminates and a satisfactory agreement was found with the experimental data.

3. Apparent in-plane stiffness properties of a single NCF lamina

The study carried out in this section aims to evaluate whether the new approach is a valid alternative for modelling the fibre crimp in NCF composites, particularly for the evaluation of the stiffness properties. Thus, the apparent in-plane stiffness properties of a single NCF lamina are predicted for different fibre crimp angles, in a range of 0º to 15º, using both modelling approaches.

The apparent in-plane stiffness equation of a single composite lamina is

$$\hat{\boldsymbol{\sigma}}_{ij}^{xy} = \bar{\boldsymbol{Q}}_{ij}\hat{\boldsymbol{\varepsilon}}_{ij}^{xy} \quad ; \quad \begin{pmatrix} \hat{\sigma}_{xx} \\ \hat{\sigma}_{yy} \\ \hat{\sigma}_{xy} \end{pmatrix} = \begin{pmatrix} \bar{Q}_{11} & \bar{Q}_{12} & \bar{Q}_{16} \\ \bar{Q}_{12} & \bar{Q}_{22} & \bar{Q}_{26} \\ \bar{Q}_{16} & \bar{Q}_{26} & \bar{Q}_{66} \end{pmatrix} \begin{pmatrix} \hat{\varepsilon}_{xx} \\ \hat{\varepsilon}_{yy} \\ \hat{\gamma}_{xy} \end{pmatrix} \tag{4}$$

where $\bar{\boldsymbol{Q}}_{ij}$ represents the lamina stiffness matrix and $\hat{\boldsymbol{\sigma}}_{ij}^{xy}$ and $\hat{\boldsymbol{\varepsilon}}_{ij}^{xy}$ represent the equivalent average stresses and strains in the lamina, respectively. The hat symbol represents the stresses and strains in the lamina and not in the tow. In this notation, *x* corresponds to the longitudinal direction of the tows and *y* to the transverse direction of the tows, so the *xy*-plane corresponds to the lamina plane, direction *z* being the through-thickness direction of the lamina. The main objective of the FE model analysis presented in this section is to predict $\bar{\boldsymbol{Q}}_{ij}$.

Notice that the notation used in expression (4) has particular connotations in this case. In general the bar indicates a reference to a nonmaterial axis system, which implies that all the terms of $\bar{\boldsymbol{Q}}_{ij}$ are different from zero. However, in this case, due to the fact that the geometric axis *x* corresponds to the nominal orientation of the fibres, the structure of $\bar{\boldsymbol{Q}}_{ij}$ is similar to that expressed in the material axis. Thus, the in-plane behaviour of each tow of the lamina is orthotropic due to the fact that all its fibres are oriented along the same direction. This idea, together with the fact that all the tows of a single lamina have the same longitudinal direction, suggests that the apparent in-plane behaviour of the lamina must be orthotropic too. This has been confirmed in view of the results obtained from the FE model, which show that the terms $\bar{Q}_{16}$ and $\bar{Q}_{26}$ of the stiffness matrix are negligible.

Once the terms of the stiffness matrix are determined, the apparent in-plane elastic moduli, E_{xx} and E_{yy}, the major Poisson's ratio ν_{xy} and the in-plane shear modulus G_{xy} of the singe NCF lamina will be calculated using the following expressions:

$$E_{xx} = \bar{Q}_{11}\left(1 - \frac{\bar{Q}_{12}^2}{\bar{Q}_{11}\bar{Q}_{22}}\right), \quad E_{yy} = \frac{\bar{Q}_{22}}{\bar{Q}_{11}}E_{xx}, \quad \nu_{xy} = \frac{\bar{Q}_{12}}{\bar{Q}_{22}}, \quad G_{xy} = \bar{Q}_{66} \tag{5}$$

3.1. Boundary conditions

The procedure that has been used to evaluate the stiffness properties of a single NCF lamina consists in applying to the FE model the appropriate boundary conditions to enable the terms of the stiffness matrix $\bar{\boldsymbol{Q}}_{ij}$ to be determined.

To determine the first column of the apparent in-plane stiffness matrix $\bar{\boldsymbol{Q}}_{ij}$, the following average strains are enforced on the model: $\hat{\varepsilon}_{xx} = \varepsilon_o$, $\hat{\varepsilon}_{yy} = 0$ and $\hat{\gamma}_{xy} = 0$. To achieve these average strains, the following displacement boundary conditions have been applied:

$$u_x = \varepsilon_o x, \text{ in faces } x = 0 \text{ and } x = a + t + g \tag{6}$$

$$u_y = 0, \text{ in all lateral faces } \left(x = 0,\ x = a + t + g,\ y = 0 \text{ and } y = a + t + g\right) \tag{7}$$

The resulting nominal stresses $\hat{\sigma}_{xx}$, $\hat{\sigma}_{yy}$ and $\hat{\sigma}_{xy}$ are calculated averaging the appropriate components of the reaction forces in the nodes of the corresponding lateral faces of the model. Eq. (4), along with the nominal values of $\hat{\varepsilon}$ and the computed values of $\hat{\sigma}$, allows the first row of the apparent in-plane stiffness matrix $\bar{\boldsymbol{Q}}_{ij}$ to be calculated.

Analogously, the second row of matrix $\bar{\boldsymbol{Q}}_{ij}$ is evaluated enforcing the average strains, $\hat{\varepsilon}_{xx} = 0$, $\hat{\varepsilon}_{yy} = \varepsilon_o$ and $\hat{\gamma}_{xy} = 0$, which results in the following displacement boundary conditions:

$$u_x = 0, \text{ in all lateral faces} \tag{8}$$

$$u_y = \varepsilon_o y \text{ in faces } y = 0 \text{ and } y = a + t + g \tag{9}$$

Finally, the third row of matrix $\bar{\boldsymbol{Q}}_{ij}$ is evaluated enforcing the average strains: $\hat{\varepsilon}_{xx} = 0$, $\hat{\varepsilon}_{yy} = 0$ and $\hat{\gamma}_{xy} = \gamma_o$, which results in the following displacement boundary conditions:

$$u_x = \frac{\gamma_o}{2} y \ , u_y = \frac{\gamma_o}{2} x, \text{ in all lateral faces.} \tag{10}$$

3.2. Results

The apparent in-plane stiffness properties, obtained with the 3D FE models of the RUC of a single NCF lamina for fibre crimp angles between 0º and 15º and employing the different modelling approaches described above, are presented in Table 3.

Maximum crimp angle (β)	Classical modelling approach				New modelling approach			
	E_{xx} (GPa)	E_{yy} (GPa)	ν_{xy}	G_{xy} (GPa)	E_{xx} (GPa)	E_{yy} (GPa)	ν_{xy}	G_{xy} (GPa)
0º	144	9.36	0.33	3.79	144	9.36	0.33	3.79
3º	143	9.36	0.32	3.79	143	9.36	0.32	3.79
6º	139	9.36	0.32	3.79	140	9.36	0.32	3.79
9º	134	9.36	0.31	3.79	136	9.36	0.32	3.79
12º	128	9.37	0.30	3.79	131	9.36	0.31	3.79
15º	121	9.37	0.30	3.79	123	9.36	0.31	3.79

Table 3. Apparent in-plane stiffness properties of a single NCF lamina for different fibre crimp angles and for the different modelling approaches.

First of all, the results show that for the evaluation of the apparent in-plane stiffness properties of a single NCF lamina with fibre crimp, a satisfactory agreement between the different modelling approaches described in Sections 2.1 and 2.2 has been found.

The numerical results show that the longitudinal elastic modulus E_{xx} and the major Poisson's ratio ν_{xy} of a single NCF lamina are slightly affected by the variation of the maximum crimp angle β. Depending on the approach used for modelling the fibre crimp, when β increases from 0º to 15º, E_{xx} and ν_{xy} decrease 14-16% and 6-9%, respectively. On the other hand, the transverse elastic modulus E_{yy} and the in-plane shear modulus G_{xy} remain almost unchanged for any of fibre crimp angles considered. The different behaviour of the elastic constants E_{xx} and E_{yy} was expected since the fibre crimp has been defined in the longitudinal through-thickness plane (*xz*-plane) of the lamina, therefore only affecting the stiffness in the nominal direction of the fibres $\left(E_{xx}\right)$.

4. Stresses and strains in global and material systems

The results obtained in the previous section show that for the evaluation of the apparent in-plane stiffness properties and therefore for the calculation of the equivalent average stresses $\hat{\boldsymbol{\sigma}}_{ij}^{xy}$ and strains $\hat{\boldsymbol{\varepsilon}}_{ij}^{xy}$ in a single NCF lamina, the geometric curvature of the tows can be replaced by a straight geometry/mesh properly defining the material properties of the tows according to the actual orientation of the fibres. It is now important to analyse whether the stresses and strains that develop along the length of the tows, in global and material systems, are also similar for both modelling approaches. These stresses and strains are of particular interest since they could be very important in the determination of the failure mode of an NCF laminate.

To analyse the stresses and strains in the tows, two equivalent RUCs of a single NCF lamina with a maximum fibre crimp angle of 15º have been generated following both modelling approaches. The boundary conditions described in (6) and (7) have been imposed on the unit cells. These boundary conditions are of special interest since they force an elongation in the fibre direction. The FE analysis has been made under the hypothesis of small displacements.

When considering these unit cells, two different areas can be clearly distinguished in the tows: one that corresponds to the straight part of the tows and another corresponding to the curved part of the tows. In the first area, the fibres within the tows are straight and consequently the stresses and strains in the longitudinal or transverse direction of the fibres have identical values in the global coordinate system *xyz* and in the material coordinate system 123, see Fig. 9(a). The stresses and strains in global and material systems will hereinafter be referred to as "nominal" and "actual" stresses/strains, respectively. In the second area, the fibres are crimped and thus the actual stresses/strains can be quite different from their nominal values, see Fig. 9(b).

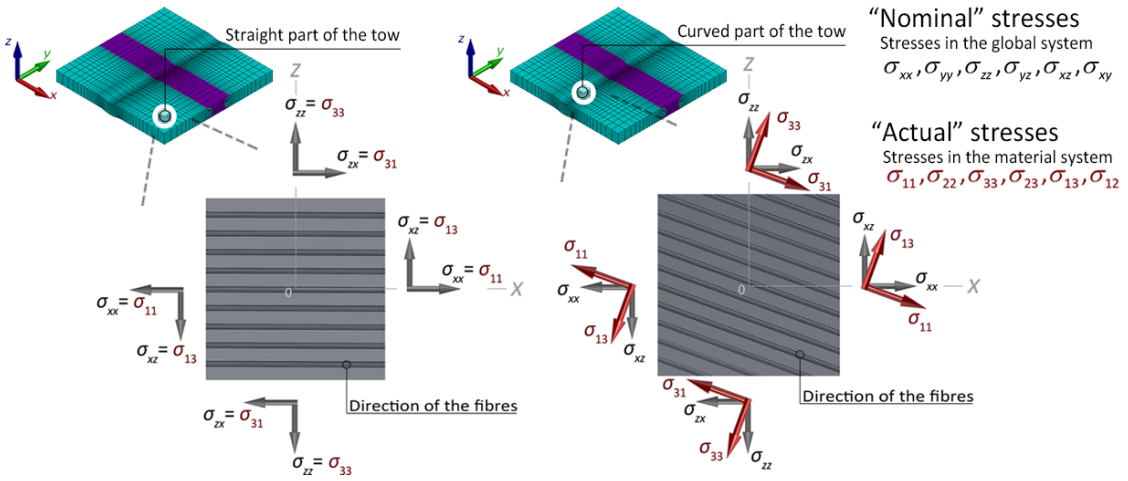

(a) (b)

Fig. 9. "Nominal" and "actual" stresses acting in the tows of a single NCF lamina: (a) in the straight part of the tows, (b) in the curved part of the tows.

Next, the nominal longitudinal stresses and strains $(\sigma_{xx}$ and ε_{xx}, respectively$)$ are compared with the averaged nominal stresses and strains $(\hat{\sigma}_{xx}$ and $\hat{\varepsilon}_{xx}$, respectively$)$ to show the influence of the presence of the resin pockets in the stresses sustained by the fibres. Also, the actual longitudinal stresses σ_{11} are compared with $\hat{\sigma}_{xx}$ and the actual longitudinal strains ε_{11} are compared with $\hat{\varepsilon}_{xx}$ to show the importance of the change in the orientation of the fibres in the tows.

The evolutions of $\sigma_{11}/\hat{\sigma}_{xx}$ and $\sigma_{xx}/\hat{\sigma}_{xx}$ along the actual direction of the fibres in the tow, represented as direction *A*, are shown in Fig. 10. Since the values of $\sigma_{11}/\hat{\sigma}_{xx}$ and $\sigma_{xx}/\hat{\sigma}_{xx}$

obtained are almost constant along the direction considered, a local scale for the ordinate axis was used (between 1 and 1.2).

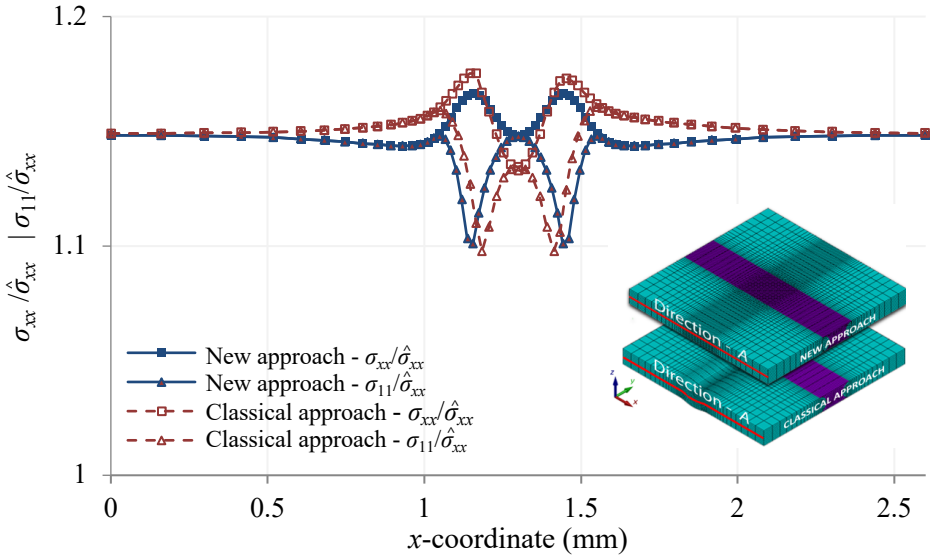

Fig. 10. $\sigma_{xx}/\hat{\sigma}_{xx}$ and $\sigma_{11}/\hat{\sigma}_{xx}$ along direction A for β=15º.

The results confirm that σ_{11} and σ_{xx} develop identically and smoothly when the fibres are straight in both FE models. It is also clear that their value is approximately 15% higher than the averaged nominal stress $\hat{\sigma}_{xx}$, which is mainly due to the presence of the resin pocket between the tows rather than to the presence of the fibre crimp. This behaviour is interrupted when the fibres start to crimp and differences between the actual and nominal stresses appear. It can be observed that independently of the modelling approach employed the increase in the misorientation angle α causes a slight reduction in σ_{11} and a slight increase in σ_{xx}. These differences are a consequence of the rotation of the stress tensor in order to express the results in the global coordinate system.

The evolutions of $\varepsilon_{11}/\hat{\varepsilon}_{xx}$ and $\varepsilon_{xx}/\hat{\varepsilon}_{xx}$ along direction A are represented in Fig. 11, in which a satisfactory agreement between the different approaches for modelling the fibre crimp can be observed.

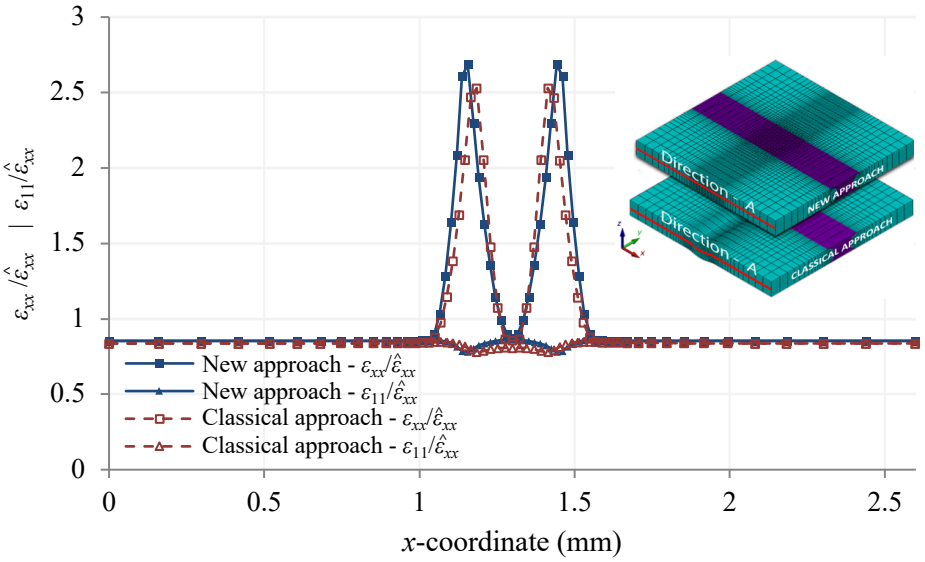

Fig. 11. $\varepsilon_{xx}/\hat{\varepsilon}_{xx}$ and $\varepsilon_{11}/\hat{\varepsilon}_{xx}$ along direction A for β=15º.

The results show that ε_{11} and ε_{xx} are identical and have a constant value (slightly inferior to the averaged nominal strain $\hat{\varepsilon}_{xx}$) when the fibres are straight, and, as expected, this behaviour is interrupted when the fibres start to crimp. While just a slight reduction is observed in the actual strains ε_{11} with the increase of the misorientation angle α, the nominal strains ε_{xx} increase by up to 270% the averaged nominal strain $\hat{\varepsilon}_{xx}$.

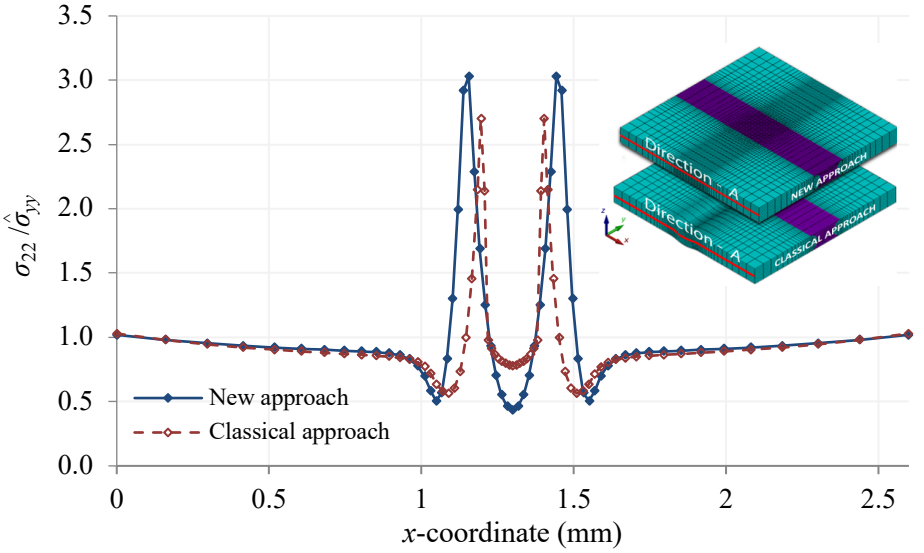

Fig. 12. $\sigma_{22}/\hat{\sigma}_{yy}$ along direction A for β=15º.

The presence of high strains ε_{xx} in the crimped part of the tows causes the appearance of high stresses in the transverse direction σ_{22} due to the Poisson's effect. The behaviour of the transverse stress σ_{22} relative to the averaged nominal transverse stress

$\hat{\sigma}_{yy}$ along direction *A*, is shown in Fig. 12. Results show that the transverse stress σ_{22} is 300% higher than the averaged nominal transverse stress $\hat{\sigma}_{yy}$ when the maximum misorientation angle α is reached.

The variation of the maximum $\sigma_{22}/\hat{\sigma}_{yy}$ is plotted versus the crimp angle β in Fig. 13.

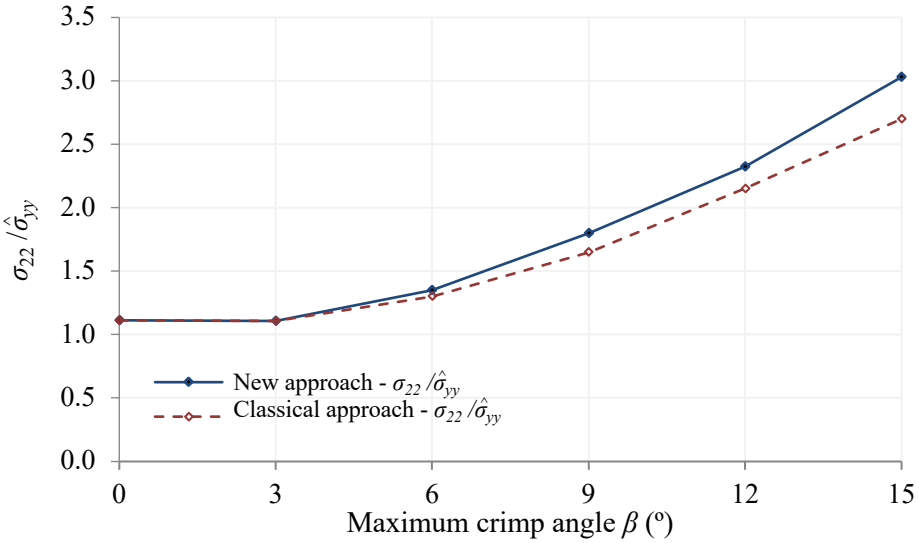

Fig. 13 – Maximum $\sigma_{22}/\hat{\sigma}_{yy}$ versus β.

Results show that for maximum crimp angles up to $\beta = 3^{\circ}$ the maximum transverse stress σ_{22} is constant and slightly higher than the averaged nominal stress $\hat{\sigma}_{yy}$ independently of the modelling approach employed. This occurs because the maximum transverse stress σ_{22} for crimp angles $\beta \leq 3^{\circ}$ is observed in the nodes with the coordinates $x = 0$ and $x = a + t + g$. For higher crimp angles the maximum transverse stress σ_{22} is localized along the crimp part of the tows, increasing almost linearly to a maximum of approximately 3 times the averaged nominal stress $\hat{\sigma}_{yy}$ (for $\beta = 15^{\circ}$).

In view of the results presented in this section, the new modelling approach can also be considered a valid alternative to study the stresses and strains that develop within the tows of NCF composites.

5. Conclusions

A new approach for modelling the fibre crimp in NCF composites has been presented. The novelty of this approach is to employ a straight 3D FE mesh. To take the fibre crimp into account an appropriate definition of the material properties in each element has to be carried out. This can be achieved either by means of an appropriate definition of anisotropic material properties in the corresponding finite elements or by the rotation of the element's coordinate system into the actual direction of the fibres.

In accordance with this new approach, 3D FE models of the RUC of a single NCF lamina with fibre crimp due to nesting of the tows have been generated. The 3D FE models have been used to evaluate numerically the apparent in-plane stiffness properties and to compare the actual and nominal stresses and strains acting in a single NCF lamina. In order to ascertain the validity of the new approach, the same studies have been performed using an equivalent RUC in which the 3D FE mesh follows the actual curvature of the tows (classical modelling approach). A satisfactory agreement has been found between the results for both FE models showing that the new approach is a valid alternative for modelling the fibre crimp in 3D FE models of NCF composites.

The advantages of the new modelling approach over the classical modelling approach are:

- Rapid modelling and meshing due to the absence of curved geometries;
- The possibility of introducing complex fibre crimps without changing the geometry/mesh of the FE model (e.g., to simulate the fibre crimp induced by the knitting process);
- A simpler geometry, which allows parametric capabilities to be added easily and higher quality meshes to obtain, thus leading to better convergence of a non-linear analysis;
- A more efficient method to generate an NCF laminate since it allows the stacking of the laminas without any interference (with no need to reposition the resin between the laminas).

Appendix A

In Section 2.1.1, Eq. (2) expresses the transformation laws for the elastic stiffness *C* and elastic compliance *S* of the material. When the transformation is a rotation of specific angle α about the *Y*-axis, the orthogonal transformation matrix is obtained by:

$$\boldsymbol{T} = \begin{pmatrix} \cos^2\alpha & 0 & \sin^2\alpha & 0 & -2\cos\alpha\sin\alpha & 0 \\ 0 & 1 & 0 & 0 & 0 & 0 \\ \sin^2\alpha & 0 & \cos^2\alpha & 0 & 2\cos\alpha\sin\alpha & 0 \\ 0 & 0 & 0 & \cos\alpha & 0 & \sin\alpha \\ \cos\alpha\sin\alpha & 0 & -\cos\alpha\sin\alpha & 0 & \cos^2\alpha-\sin^2\alpha & 0 \\ 0 & 0 & 0 & -\sin\alpha & 0 & \cos\alpha \end{pmatrix} \tag{A.1}$$

The following contracted notation has been employed to define the stresses, σ, and strains, ε, in the global coordinate system and the stresses, σ^*, and strains, ε^*, in the local coordinate system.

$$\sigma = \{\sigma_{xx}, \sigma_{yy}, \sigma_{zz}, \sigma_{yz}, \sigma_{xz}, \sigma_{xy}\}^T,\ \varepsilon = \{\varepsilon_{xx}, \varepsilon_{yy}, \varepsilon_{zz}, \gamma_{yz}, \gamma_{xz}, \gamma_{xy}\}^T$$
$$\sigma^* = \{\sigma_{11}, \sigma_{22}, \sigma_{33}, \sigma_{23}, \sigma_{13}, \sigma_{12}\}^T,\ \varepsilon^* = \{\varepsilon_{11}, \varepsilon_{22}, \varepsilon_{33}, \gamma_{23}, \gamma_{13}, \gamma_{12}\}^T \quad \text{(A.2)}$$

Appendix B

The apparent stiffness properties of the tows in the longitudinal planes $\left(E_{11}^t,\ \nu_{12}^t \text{ and } G_{12}^t\right)$ and the transverse planes $\left(E_{22}^t,\ \nu_{23}^t \text{ and } G_{23}^t\right)$ have been estimated from the resin stiffness properties $\left(E^m,\ \nu^m \text{ and } G^m\right)$ and the stiffness properties of the fibres in the longitudinal plane $\left(E_{11}^f,\ \nu_{12}^f \text{ and } G_{12}^f\right)$, using the rule of mixtures. The longitudinal elastic modulus E_{11}^t, the transverse elastic modulus E_{22}^t, the Poisson's ratio ν_{12}^t, the longitudinal shear modulus G_{12}^t and the transverse shear modulus G_{23}^t are interpolated using the following expressions:

$$\begin{aligned}
E_{11}^t &= E_{11}^f V_f^t + E^m V_m^t \\
E_{22}^t &= \frac{E_{11}^f E^m}{E_{11}^f V_m^t + E^m V_f^t} \approx \frac{E^m}{V_m^t} \\
\nu_{12}^t &= \nu_{12}^f V_f^t + \nu^m V_m^t \\
G_{12}^t &= G_{23}^t = \frac{G_{12}^f G^m}{G_{12}^f V_m^t + G^m V_f^t} \approx \frac{G^m}{V_m^t}
\end{aligned} \quad \text{(B.1)}$$

with, V_f^t and V_m^t being, respectively, the fibre and matrix volume fraction in the tow. Finally, the Poisson's ratio in transverse planes has been estimated from the isotropic conditions,

$$\nu_{23}^t = \frac{E_{22}^t}{2G_{23}^t} - 1 \quad \text{(B.2)}$$

References

[1] Bibo GA, Hogg PJ, Kemp M. Mechanical characterisation of glass- and carbon-fibre-reinforced composites made with non-crimp fabrics. Composites Science and Technology. 1997;57:1221-41.

[2] Shyr T-W, Pan Y-H. Impact resistance and damage characteristics of composite laminates. Composite Structures. 2003;62:193-203.

[3] Miller AJ. The effect of microstructural parameters on the mechanical properties of non-crimp fabric composites [M. Phil thesis]: Cranfield University, School of Industrial and Manufacturing Science, 1996.

[4] Kong H, Mouritz AP, Paton R. Tensile extension properties and deformation mechanisms of multiaxial non-crimp fabrics. Composite Structures. 2004;66:249-59.
[5] Mattsson D, Joffe R, Varna J. Methodology for characterization of internal structure parameters governing performance in NCF composites. Composites Part B-Engineering. 2007;38:44-57.
[6] Drapier S, Wisnom MR. A finite-element investigation of the interlaminar shear behaviour of non-crimp-fabric-based composites. Composites Science and Technology. 1999;59:2351-62.
[7] Drapier S, Wisnom MR. Finite-element investigation of the compressive strength of non-crimp-fabric-based composites. Composites Science and Technology. 1999;59:1287-97.
[8] Joffe R, Mattsson D, Modniks J, Varna J. Compressive failure analysis of non-crimp fabric composites with large out-of-plane misalignment of fiber bundles. Composites Part a-Applied Science and Manufacturing. 2005;36:1030-46.
[9] París F, González A, Graciani E, Flores M, Castillo E. A 3D FEM study of compressive behaviour of non-crimp fabrics. In: 11th European conference on composite materials (ECCM11). Rhodes, Greece 2004.
[10] Carvelli V, Truong T, Larosa MS, Lomov SC. Experimental and numerical determination of the mechanical properties of multi-axial multi-ply composites. In: 11th European Conference on Composite Materials. Rhodes, Greece 2004.
[11] Gonzalez A, Graciani E, París F. Prediction of in-plane stiffness properties of non-crimp fabric laminates by means of 3D finite element analysis. Composites Science and Technology. 2008;68:121-31.
[12] Hess H, Himmel N. Structurally stitched NCF CFRP laminates. Part 2: Finite element unit cell based prediction of in-plane strength. Composites Science and Technology. 2011;71:569-85.
[13] Marklund E, Asp LE. Multiscale methodology for matrix failure prediction in non-crimp fabric composites. In: 14th European Conference on Composite Materials. Budapest, Hungary 2010.
[14] Mattsson D, Joffe R, Varna J. Damage in NCF composites under tension: Effect of layer stacking sequence. Engineering Fracture Mechanics. 2008;75:2666-82.
[15] Oakeshott JL, Iannucci L, Robinson P. Development of a representative unit cell model for bi-axial NCF composites. Journal of Composite Materials. 2007;41:801-35.
[16] Tserpes KI, Labeas GN. Mesomechanical analysis of non-crimp fabric composite structural parts. Composite Structures. 2009;87:358-69.
[17] Joffe R. Characterization of performance. Performance in tension. Elastic properties and failure. FALCOM/WP3:T3.2.1/LTU. 2004.
[18] Mattsson D, Joffe R, Varna J. Characterisation of processability and manufacturing. Characterisation of microstructure. FALCOM/WP2:D2.1-4/LTU. 2004.
[19] ANSYS. Release 11.0 documentation. Swanson Analysis Systems Inc 2008.
[20] Lekhnitskii SG, Fern P, Brandstatter JJ, Dill EH. Theory of Elasticity of an Anisotropic Elastic Body. Physics Today. 1964;17:84.

[21] Graciani E, González A, París F. Análisis del comportamiento a compresión de un laminado [0,90,0,90] de tejido no ondulado mediante un modelo 3D de elementos finitos. In: Materiales Compuestos 05 Editorial de la UPV.; 2005. p. 877-84.
[22] Potluri P, Thammandra VS. Influence of uniaxial and biaxial tension on meso-scale geometry and strain fields in a woven composite. Composite Structures. 2007;77:405-18.
[23] Joffe R. Performance of non-crimp fabric composites in shear. Trends in Composite Materials and Their Design. 2010;425:45-59.